

Progress on the experimental set-up for the testing of a floating offshore wind turbine scaled model in a field site

C. Ruzzo¹, V. Fiamma¹, V. Nava², M. Collu³, G. Failla¹, and F. Arena¹

¹*Mediterranea University, Natural Ocean Engineering Laboratory, Reggio Calabria, Italy, carlo.ruzzo@unirc.it, vincenzo.fiamma@unirc.it, giuseppe.failla@unirc.it, arena@unirc.it,*

²*Tecnalia Research & Innovation, Energy and Environment Division, Bilbao, Spain, vincenzo.nava@tecnalia.com*

³*Cranfield University, Cranfield, United Kingdom, maurizio.collu@cranfield.ac.uk*

Abstract – This document describes the design and the realization of a small scale field experiment on a 1:30 model of a spar floating support structure for offshore wind turbines. The aim of the experiment is to investigate the dynamic behaviour of the floating wind turbine under extreme wave and parked rotor conditions. The experiment has been going on in the Natural Ocean Engineering Laboratory (NOEL) of Reggio Calabria (Italy). In this paper all the stages of the experimental activity are presented and some results are shown in terms of motions and RAOs. Finally, a comparison with the corresponding results obtained using the ANSYS AQWA software package is shown and conclusions are drawn. The herein presented experimental set up seems promising to test offshore floating structures for marine renewable energy at a relatively large scale in the NOEL field site.

Keywords – Spar, floating wind turbines, sea experiment, intermediate scale model

1. Introduction

Offshore wind is one of the most promising sources of renewable energy (see e.g. Failla & Arena, 2015). Offshore sites feature relevant advantages over onshore ones, as there are generally higher wind speeds and lower turbulence, larger areas available for large scale wind farms, lower visual impact at distance from the shore. Current typical design involves three-bladed, upwind rotors with horizontal axis, mounted on a support structure composed of a tower resting on a bottom-fixed substructure, or a floating device moored to the seabed. Fixed supports as monopiles, tripods and jackets are adopted for water depths lower than 50 m but, as water depth increases, floating ones seem to be a technically feasible and more economically viable option [2-10]. Various floating devices have been proposed, usually classified based on the primary physical principle adopted to achieve static stability: the spar-buoy, whose stability is provided by a ballast lowering the centre of gravity below the centre of buoyancy; the tension leg platform (TLP), where stability is achieved via mooring lines kept under tension by excess buoyancy in the platform [7]; the barge and the semi-submersible, where stability is achieved mainly through the waterplane area [2-8]. The spar-buoy, barge and semi-submersible configurations are generally moored by catenary lines. Hybrid concepts using features from the three classes are also under study.

Among the others, the spar concept seems to be particularly suitable for ultra-deep water. It consists of a slender hollow cylinder, placed in vertical position and ballast-stabilized. The technical feasibility of floating wind turbines on a spar support has been already demonstrated

by the 2.3 MW Hywind turbine prototype installed by StatoilHydro off the south-west coast of Norway, at a water depth of about 200 m [11-12]. Furthermore, reference full-scale design examples have been provided by the OC3-Hywind spar coupled with the NREL-5MW wind turbine, developed within the Offshore Code Comparison Collaboration (OC3) project [13-15], and by the UMaine-Hywind demonstration project [9].

Most model tests of floating wind turbines on spar supports have been conducted in ocean basin facilities with wave generators [16-19]. A few model tests have been deployed or are currently in planning stages also at intermediate scale in sea water, promoted by commercial and public entities. Examples are a 1:5 scale test of a tension-leg spar design in Norway, a 1:2 scale 100-kW spar in Japan. An overview on intermediate scale tests of floating offshore wind turbines currently going on is given in ref. [20]. Data is still limited, but these programs corroborate the interest in conducting intermediate scale tests prior to full-scale projects. The main advantage of intermediate scale is that hydrodynamic properties of the models are closer to those of the corresponding full scale structures respect to smaller scale experiments, especially relatively to viscous forces, since the models are usually Froude scaled. On the other hand, the costs associated with these tests increase substantially and it is often difficult to find suitable sites.

Considerable effort has been devoted to compare experimental tests with numerical simulations. An overview of the numerical codes to perform a fully-coupled analysis considering dynamics from wave, structure and wind may be found in ref. [21]. A first important step is, however, to compare the numerical predictions of the hydrodynamic response of the floating wind turbine system with the experimental results, considering a zero wind speed. In this context, a comparison between experimental results on a spar support in a wave tank and numerical simulation by ORCAFLEX was presented in ref. [19]. Skaare et al. [22] compared the experimental response of scale model of the Hywind spar with the response of a numerical model in SIMO/RIFLEX. Experimental results of scale models of the OC3-Hywind spar were compared with those from numerical models implemented in 3Dfloat and ANSYS by Myhr et al. [23], in aNySIM by Gueydon et al. [24].

This paper presents the preliminary results of experimental tests on a 1:30 scale model of the UMaine-Hywind spar, carried out in sea water at the Natural Ocean Engineering Laboratory (NOEL) of Reggio Calabria. A first stage plan of the experimental activity was presented in ref. [25]. In the present work the final design is presented and the preliminary experimental results are compared with the numerical results from ANSYS AQWA [26]. Testing in sea water will allow the scale model of the UMaine-Hywind spar to be validated at a larger scale than the usual ones possible in wave basins, thus obtaining more reliable information on its dynamic behaviour. The model has been scaled following a Froude similitude whenever possible, fulfilling nonetheless the structural resistance requirements imposed by the loads experienced at this scale. At this stage of the experimental activity, only the hydrodynamics is studied; the turbine is considered in parked position and is represented by a lumped mass at the top.

2. Scaling features

2.1 The NOEL facilities

The experiment is being realized in the NOEL Laboratory, which is located in the South of Italy, off the beach of Reggio Calabria, as shown in Figure 1.

Thanks to the unique local environmental characteristics, such as the low variability of the local wind, the orientation of the coast and the relatively short fetch, this site is particularly

suitable to represent severe ocean conditions at these intermediate model scales. A more exhaustive description of the site characteristics and of its advantages with respect to conventional sites can be found in ref. [27]. Typical sea states occurring at NOEL have significant wave height between 0.20 and 0.40 m, peak periods between 1.8 and 2.6 s, and JONSWAP-like spectra, representing excellent small scale models, in Froude similarity, of severe ocean sea storms. An example of sea-state recorded at NOEL, fulfilling these requirements, is shown in Figure 2. Boccotti's approach [27] has been followed and normalized spectra of wave surface elevation and wave head of pressure at a depth of 0.97 m have been plotted and compared to make sure that there is no swell component, which would affect significantly Froude similarity. The significant wave height for this sea-state is 0.30 m and the peak period is 2.5 s.

The local seabed is inclined with almost constant slope and is equipped with a dense grid of anchors. Water depth varies from 0 to about 18m and maximum tidal amplitude is of the order of few tens of centimetres.

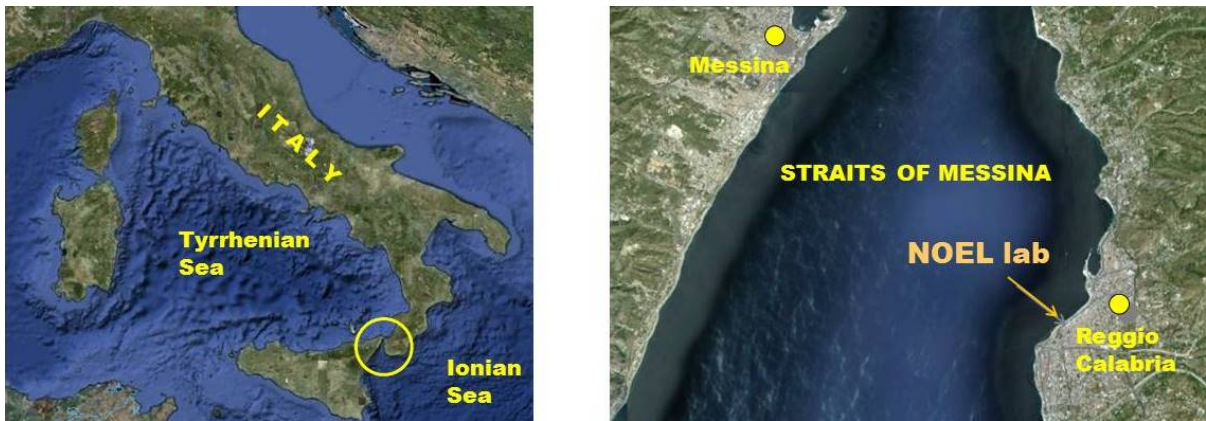


Figure 1: Location of Natural Ocean Engineering Laboratory (LAT: 38°06.538'N; LONG: 15°38.478E).

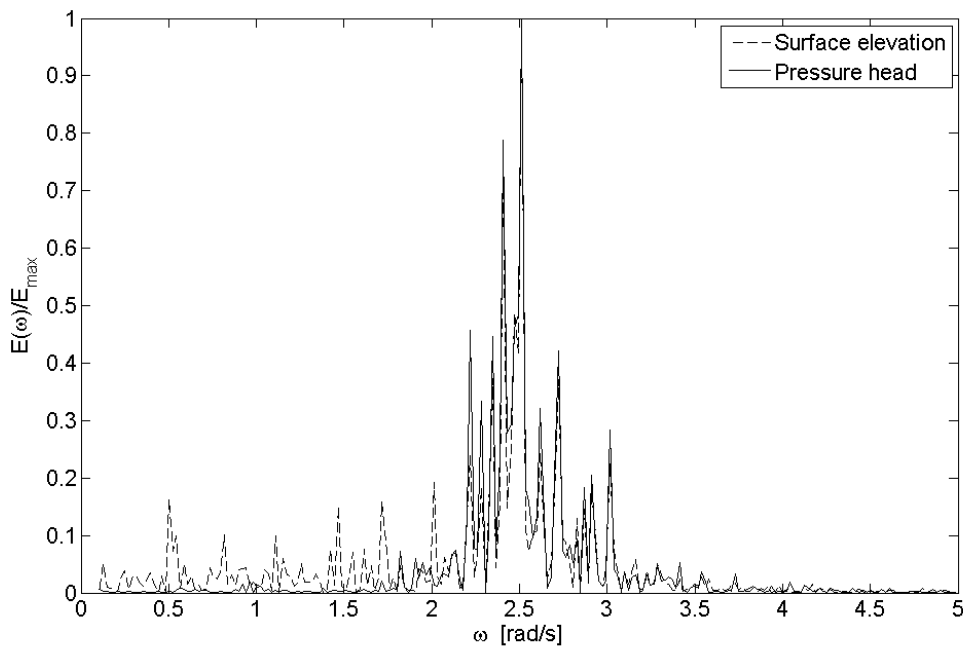


Figure 2: Example of pure wind waves spectrum.

2.2 Influence of the scale factor

Due to the choice of representing the ultimate wave conditions of the prototype, a scale factor of 30 has been adopted. Indeed, a local sea state with significant wave height of 0.30 m is representative of a strong sea storm with $H_s = 9.0$ m, which well represents ultimate load conditions for the Mediterranean climate. This choice of the scale factor is crucial for the adequate scaling of hydrodynamic forces on the spar structure.

Wave loads on slender cylinders can be calculated by means of Morison Equation (see e.g. ref. [28]):

$$f_N = \rho_w A a + \rho_w C_A A a_r + \frac{1}{2} \rho_w C_D |v_r| v_r \quad (1)$$

being ρ_w the seawater density, A the cross-sectional area of the cylinder, a the water particle acceleration, v_r , the relative velocity between fluid and structure, a_r the relative acceleration, C_A the added mass coefficient and C_D the drag coefficient. The hydrodynamic coefficients depend on Keulegan-Carpenter number and Reynolds number, which are given by:

$$K_C = \frac{v_{\max} T}{D} \quad (1)$$

$$R_e = \frac{v_{\max} D}{\nu} \quad (2)$$

being v_{\max} the maximum horizontal water particle velocity, D the diameter of the cylinder, T the wave period and ν the water cinematic viscosity. For wave loading in random waves [29] the wave period and water particle velocity could be respectively taken as the zero-up-crossing period T_z and:

$$v_{\max} = \sqrt{2} \sigma_v \quad (3)$$

being σ_v the standard deviation of the fluid velocity.

Experimental activities were already carried out in the NOEL Laboratory to determine the hydrodynamic coefficients of Morison equation in irregular waves [30-31]. Table 1 summarizes Froude scaling laws and it can be noted that the Reynolds number is inevitably lower for a small scale model and hydrodynamic coefficients are hence altered. However, according to many authors [30-32] the effect of this change on hydrodynamic coefficients can be neglected as long as the following condition is satisfied:

$$\frac{R_e}{K_C} = \frac{D^2}{T} > 10^4 \quad (4)$$

The scale factor chosen allows to satisfy condition (4) for all relevant wave conditions, as it is shown in Table 2, where the comparison with a smaller (1:60) model is also shown. As it can be seen, the possibility of working at a relatively large scale respect to conventional ocean basin experimental activities, guarantees more reliable scaling, especially concerning ultimate wave conditions, where nonlinear (e.g. drag) forces are more important.

Table 1: Froude Scaling laws.

Parameter	Units	Scale factor
Length	[m]	λ
Time	[s]	$\lambda^{0.5}$
Density	[kgm ⁻³]	1
Velocity	[ms ⁻¹]	$\lambda^{0.5}$
Acceleration	[ms ⁻²]	1
Mass	[kg]	λ^3
Mass moment of inertia	[kgm ²]	λ^5
Force	[N]	λ^3
Keulegan-Carpenter	[-]	1
Reynolds	[-]	$\lambda^{1.5}$

Table 2: Comparison between two scale factors in terms of condition (4) at the SWL.

Full scale sea state		1: 30 scale model			1: 60 scale model		
H_s	T_z	H_s	T_z	R_e/K_C	H_s	T_z	R_e/K_C
3 m	7.4 s	0.10 m	1.05 s	$4.4 \cdot 10^4$	0.05 m	0.95 s	$1.6 \cdot 10^4$
6 m	10.4 s	0.20 m	1.49 s	$3.2 \cdot 10^4$	0.10 m	1.35 s	$1.1 \cdot 10^4$
9 m	12.8 s	0.30 m	1.82 s	$2.6 \cdot 10^4$	0.15 m	1.65 s	$0.9 \cdot 10^4$
12 m	14.8 s	0.40 m	2.10 s	$2.2 \cdot 10^4$	0.20 m	1.91 s	$0.8 \cdot 10^4$

3. Description of the Experimental Setup

3.1 Description of the model structure

The UMaine-Hywind spar buoy is the concept chosen for the present analysis. It consists of a steel tapered cylinder moored through three catenary lines. Detailed description of the support structure can be found in [9,14]. It should be noted that UMaine-Hywind support structure and wind turbine are the same of the OC3-Hywind reference project, but it differs for the mooring system, which is designed for a lower water depth. The most important characteristics of UMaine-Hywind are summarized in the first column of Table 3.

The design of the small scale model has been done so that geometry, masses and moments of inertia are scaled according to Froude similarity. However, being the installation site a non-controlled environment, local extreme climate can occasionally exceed any condition usable for the experiment. As a consequence, structural resistance of the model has been oversized, keeping total mass and moments of inertia of the model as close as possible to those of the scaled UMaine-Hywind.

In detail, wall thickness of the steel cylinder has been augmented, and the consequent increases in weight and centre of gravity height have been counterbalanced by substituting water and rock ballast with steel discs, placed in the lower part of the hull. In such a way, the overall position of the centre of gravity has been preserved while the change in mass distribution involves an alteration of mass moments of inertia, which has been partially adjusted by adjusting the design of the tower and RNA masses. Since the measurement station efficiency is strongly affected by the proximity of ferromagnetic materials, the tower has been manufactured in aluminium and the station has been placed on its top. The necessary tower structural stiffness

has been achieved through a tubular section with a diameter of 100 mm and a wall thickness of 5 mm. The RNA has been represented with a fixed aluminium plate with a mass of 8.7 kg.

The most important characteristics of the model structure are summarized in the third column of Table 3 and compared with those of the full scale structure. The hull of the model (before and after the installation) and the tower are shown in Figure 3. The installation took place in July 2015 and the experiment is currently going on.

Table 3: Main characteristics of the support structure at prototype and model scale.

Parameter	UMaine-Hywind (1:1)	UMaine-Hywind (1:30)	Model (1:30)
Water depth	200 m	6.67 m	6.90 m (spar)
Total spar length	130 m	4.333 m	4.334 m
Spar draft	120 m	4.000 m	4.001 m
Upper spar diameter	6.50 m	0.217 m	0.217 m
Lower spar diameter	9.40 m	0.313 m	0.313 m
Spar ballasted mass	$7.466 \cdot 10^6$ kg	276.5 kg	275.3 kg
Spar centre of gravity (above keel level)	30.08 m	1.003 m	1.031 m
Tower height	80 m	2.67 m	2.60 m
Overall Mass	$8.066 \cdot 10^6$ kg	298.7 kg	296.2 kg
Overall centre of gravity (height above keel)	42.00 m	1.400 m	1.381 m
Mass moments of inertia I_{xx}, I_{yy} (respect to SWL)	$6.803 \cdot 10^{10}$ kgm ²	$2.799 \cdot 10^3$ kgm ²	$2.976 \cdot 10^3$ kgm ²
Mass moment of inertia I_{zz}	$1.916 \cdot 10^8$ kgm ²	7.860 kgm ²	4.861 kgm ²

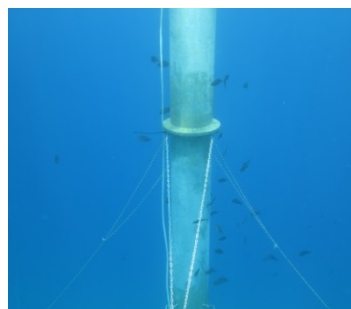


Figure 3: Installation phases of the structure: hull before and after installation, instrumented tower.

3.2 Description of the mooring system

The design of the mooring lines has been modified with respect to that of the full scale structure in order to take into account the slope of the local seabed. In particular, with respect to the equilibrium spar position, the anchor on the land side is placed at a lower water depth, while the two anchors on the sea side are placed at a higher one.

In the design phase, a simplified 2D quasi-static approach has been adopted. Under the hypothesis of an inextensible catenary line with touchdown, catenary equation can be written as:

$$z(x) = \frac{T_h}{p} \cosh \left[\frac{p}{T_h} x + \operatorname{arcsen} h[\tan(\beta)] \right] - \frac{T_h}{p} \sqrt{1 + \tan^2(\beta)} \quad (5)$$

being p the weight per unit length of the line, T_h its horizontal tension and β the slope of the seabed and Oxz a reference system centred in the touchdown point O . The unknown T_h and the shape of the line, can be obtained by the numerical solution of a nonlinear system of three equations, given by the imposition of the opportune boundary conditions, depending only on the relative positions of the anchor point and the fairlead of the structure, in its equilibrium position.

In order to minimize the differences in surge and sway behaviour of the model with respect to those of the full scale structure, each line would have been designed such that the equivalent stiffness of the line is properly scaled. However, due to the non controlled environment, it has been chosen to slightly increase the lines length, thus reducing equivalent stiffness, to guarantee a proper behaviour of the model structure also in local extreme conditions. The most important characteristics of the mooring line system are presented in Table 4, while their shapes in equilibrium position are shown in Figure 4.

Delta connection of the mooring lines has been realized in order to reduce the yaw motion of the support structure, following the practical suggestions given by Quallen et al. [33] for the design, i.e. each delta segment is long about a tenth of the mooring line.

Table 4: Main characteristics of the mooring system at prototype and model scale.

Parameter	UMaine-Hywind (1:1)	UMaine-Hywind (1:30)	Model (1:30)
Sea-side anchor depth	200 m	6.67 m	10.40 m
Land-side anchor depth	200 m	6.67 m	2.75 m
Fairleads depth	70 m	2.333 m	2.341 m
Linear mass	145 kgm ⁻¹	0.161 kgm ⁻¹	0.159 kgm ⁻¹
Radius sea-side anchor – spar centerline	445 m	14.83 m	14.00 m
Radius land-side anchor – spar centerline	445 m	14.83 m	13.00 m
Pretension sea-side line	8.673·10 ⁵ N	32.12 N	31.76 N
Pretension land-side line	8.673·10 ⁵ N	32.12 N	25.51 N
Sea-side line length	468 m	15.60 m	16.50 m
Land-side line length	468 m	15.60 m	13.30 m

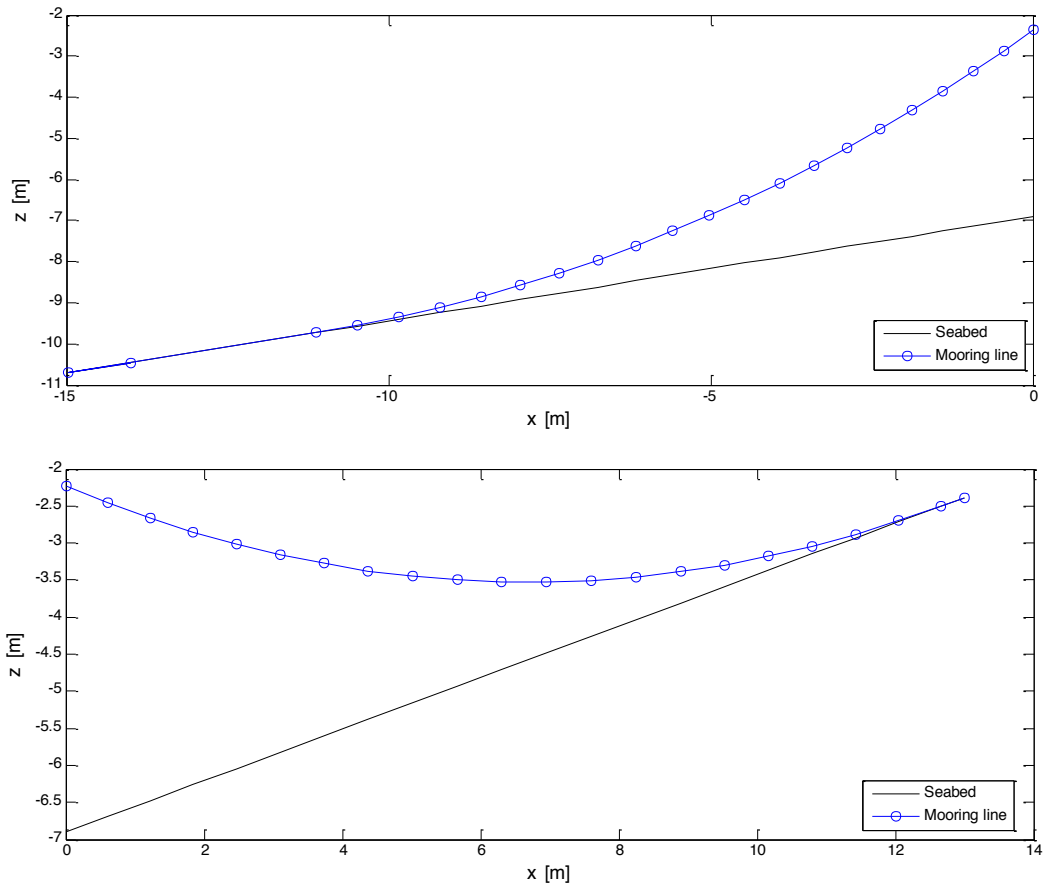


Figure 4: Catenary shape in the equilibrium position: sea-side (top); land-side (bottom).

3.3 Numerical validation of the small scale model

The validation of the small scale model design has been done by numerical simulations in frequency domain, using the commercial software ANSYS AQWA.

The proper modelling of hydrodynamic properties of OC3 Hywind has been intensively discussed by Jonkman [14]. In this work, he suggests two equivalent approaches for the modelling of the full scale structure. The first one is based solely on the Morison equation, whose hydrodynamic coefficients should be chosen such that added mass equals the zero-limit in frequency of surge added mass from potential theory and drag coefficient equals the asymptotical value for condition (4). The resulting coefficients in this case are $C_A \approx 0.97$ and $C_D \approx 0.60$. Equivalently, the second approach is based on the potential theory, with the addition of the drag term of Morison equation, in order to take into account the nonlinear damping due to flow separation in surge, sway, roll and pitch motions, which is relevant in severe ocean conditions. Both approaches have been implemented in AQWA and results are very close to each other and to those obtained by Ramachandran et al. [34]. In this paper, the latter approach has been chosen.

Following the instructions of Jonkman, due to the experience matured in the Hywind project by Statoil [11-12], the sum of linear radiation and nonlinear viscous damping is not sufficient to represent the whole damping properties of the platform. Hence, additional frequency-independent linear damping matrix has been inserted in the model of the full scale structure. The terms of this matrix are reported in Table 5. Since an accurate hydrodynamic identification of the model has not been conducted yet due to the difficulty of conducting free

decay tests in the open sea location, the same matrix has been adopted also in the numerical analysis of the small scale model.

Since the commercial software used is not able to represent the complex catenary mooring system of the small scale model, an equivalent mooring system in horizontal seabed conditions has been considered, with the same pretension at the fairleads. As a result the non-linear cable stiffness results overestimated in the case of finite surge and sway motions, resulting in slightly higher natural frequencies and lower numerical motions in the translational degrees of freedom than those expected during the experiment. Additional linear stiffness in yaw motion has been inserted both for small and full scale structures to take into account the delta connections of the mooring lines (see Table 5).

Table 5: Additional linear hydrodynamic properties.

Damping in surge and sway motions	$1.0 \cdot 10^5 \text{ Nsm}^{-1}$
Damping in heave motion	$1.3 \cdot 10^5 \text{ Nsm}^{-1}$
Damping in yaw motion	$1.3 \cdot 10^7 \text{ Nms}$
Stiffness in yaw motion	$9.8 \cdot 10^7 \text{ Nm}$

The comparison between RAOs of UMaine-Hywind and the small scale model, both presented at the full scale, is shown in Figures 5-7. These RAOs include the effects of mooring lines dynamics and Morison drag, which have been linearized for a conventional sea state, having $H_s = 6.0 \text{ m}$, $T_p = 10.0 \text{ s}$, mean propagation direction along x axis and mean-JONSWAP spectrum. The linearization procedure is explained in the theory manual of ANSYS AQWA [35]. The comparison between natural frequencies is shown in Table 6. As expected, good agreement is obtained, except for horizontal motions natural frequencies, which are slightly overestimated. In conclusion, we can observe that the small scale model represents well the hydrodynamic behaviour of the structure.

Table 6: Natural frequencies comparison at the full scale between UMaine-Hywind and the ANSYS AQWA model.

Mode	UMaine-Hywind (1:1)	Model (1:1)	Model (1:30)
Surge – Sway	0.048 rad/s	0.062 rad/s	0,342 rad/s
Heave	0.195 rad/s	0.201 rad/s	1,101 rad/s
Roll – Pitch	0.210 rad/s	0.201 rad/s	1,101 rad/s
Yaw	0.766 rad/s	0.903 rad/s	4,956 rad/s

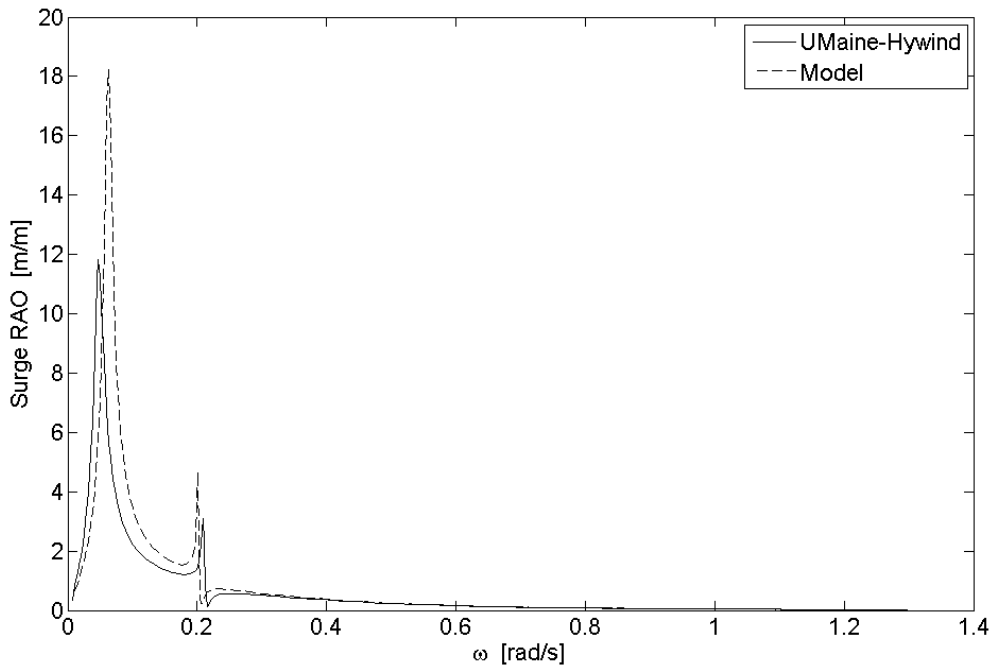


Figure 5: Surge RAO comparison at the full scale between UMaine-Hywind and the ANSYS AQWA model.

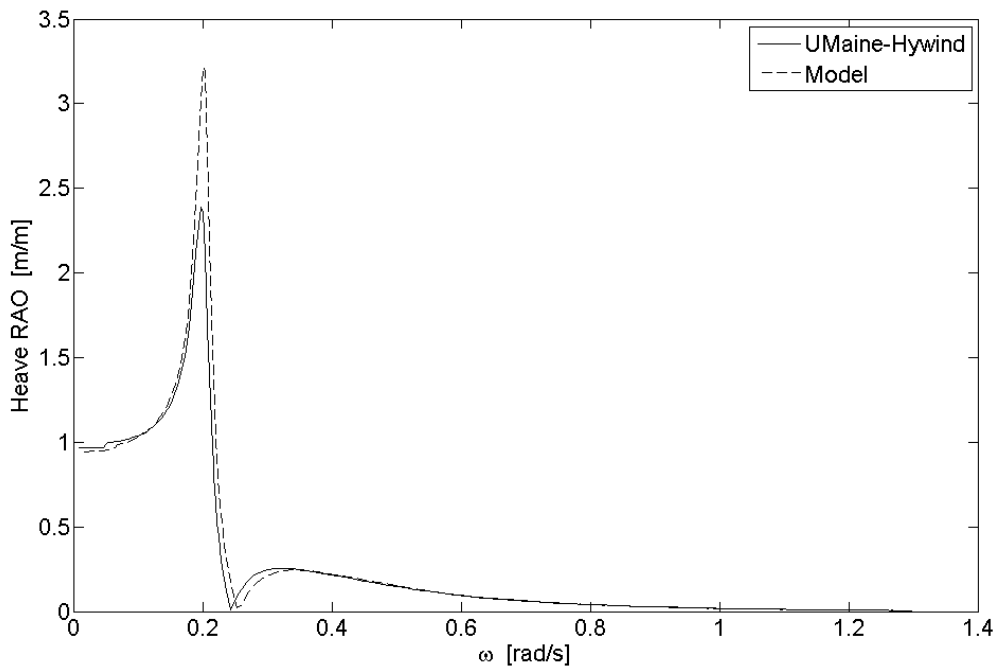


Figure 6: Heave RAO comparison at the full scale between UMaine-Hywind and the ANSYS AQWA model.

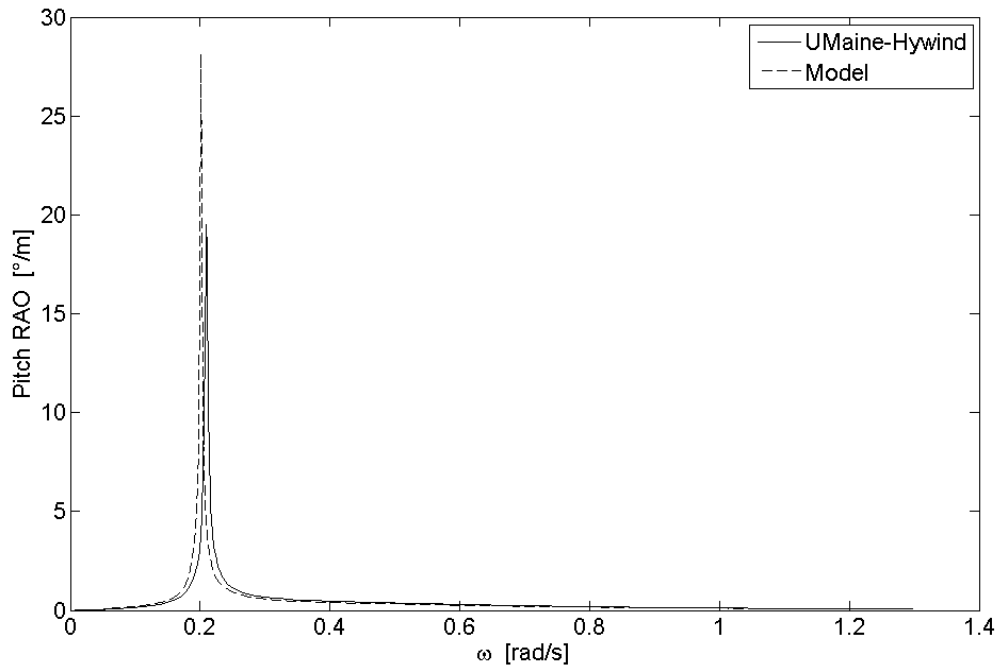


Figure 7: Pitch RAO comparison at the full scale between UMaine-Hywind and the ANSYS AQWA model.

4. Experimental Results

4.1. Description of the measuring equipment

Measuring equipment consists of:

- A Real-Time Kinematic Differential Global Positioning System (RTK DGPS), placed at the top of the tower, used to measure body motion along North, East and vertical directions;
- An inertial measurement unit (AHRS), placed at the top of the tower, used to measure body motion in yaw, pitch (defined as the rotation around East) and roll (defined as the rotation around North) ;
- Two wave measurement stations, each made up of an ultrasonic probe for measuring wave elevation and a pressure transducer for more accurate measure of the wave pressure head. Both the stations are placed few meters far from the spar at a water depth of about 2.16 m. The pressure transducers are placed 1.05 m above the seabed.

4.2 Experimental data

Since the installation of the model, 765 five-minutes long sea states and corresponding spar motions have been recorded. Significant wave height and tidal amplitude are calculated from the elevation data of the ultrasonic probes while dominant wave direction, as well as wave spectrum, is obtained from pressure data, following the method proposed in ref. [27]. Maximum measured tidal amplitude is about 0.20 m, hence its effect on the spar and anchors water depths is negligible for the scope of this work.

Within the entire database of records, only wind generated sea states and related structure

motions have been selected, resulting in 138 data. Following Boccotti's approach [27], the selection process is based on the condition $\psi^* > 0.8$, being ψ^* , the narrow-bandedness parameter of wave pressure head spectrum.

Since the wave dominant direction is not constant, surge has been conventionally identified as the translation along the North-South direction (positive toward North), while sway as the one along the East-West direction (positive toward East). Consistently, roll has been defined as the rotation about North-axis and pitch as the rotation about East-axis. Heave has been conventionally defined as the translation along z-axis (positive upward) and yaw as the rotation about it.

In Figures 8-11 significant motions in all degrees of freedom versus significant wave height are shown. Only sea states with a dominant propagation direction within $[20^\circ, 40^\circ]$ with respect to North are considered, resulting in 85 data.

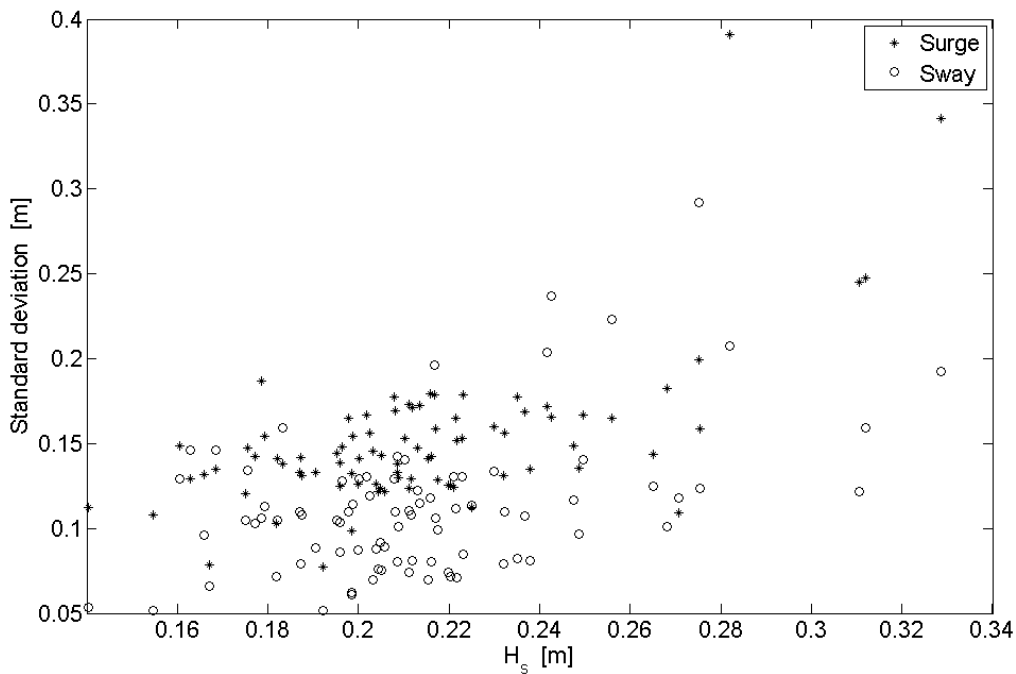


Figure 8: Significant motions of the model in surge and sway at the tower top versus significant wave height.

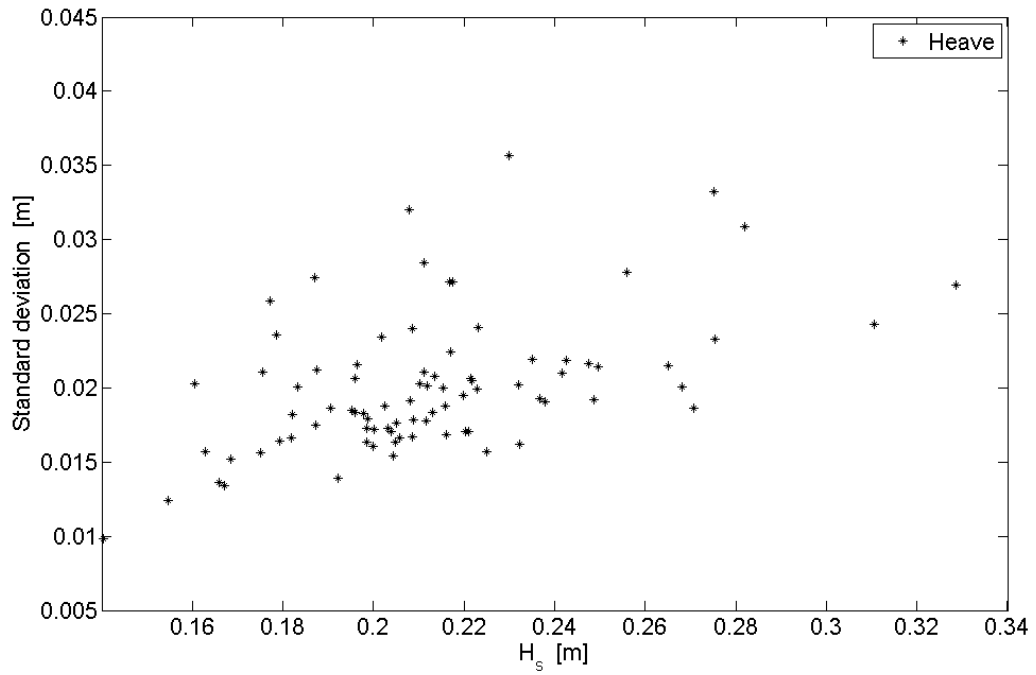


Figure 9: Significant motions of the model in heave at the tower top versus significant wave height.

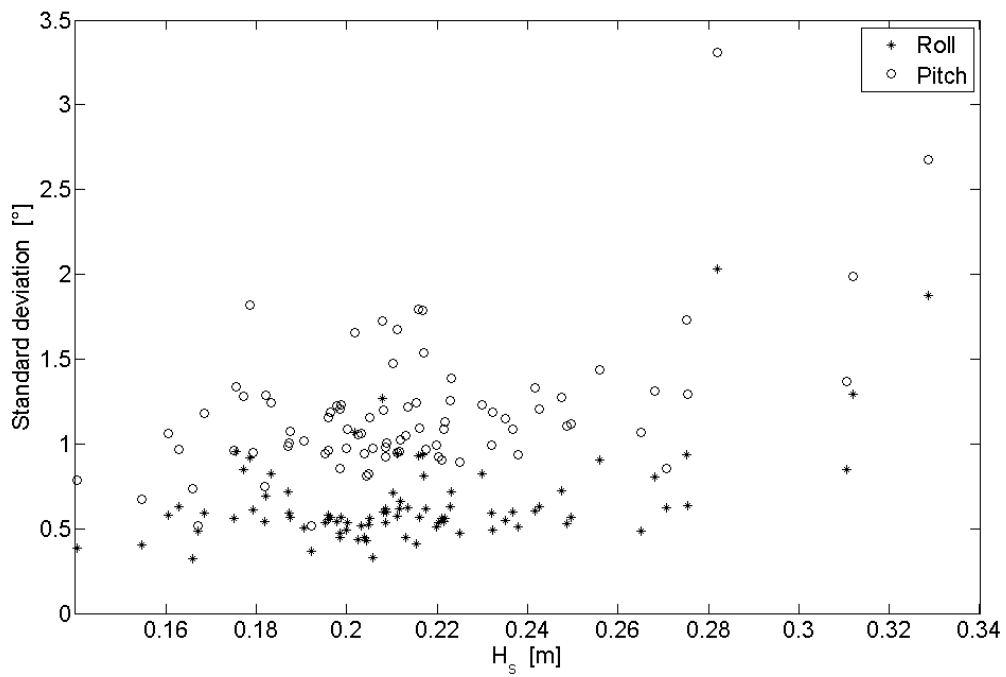


Figure 10: Significant motions in the model roll and pitch versus significant wave height.

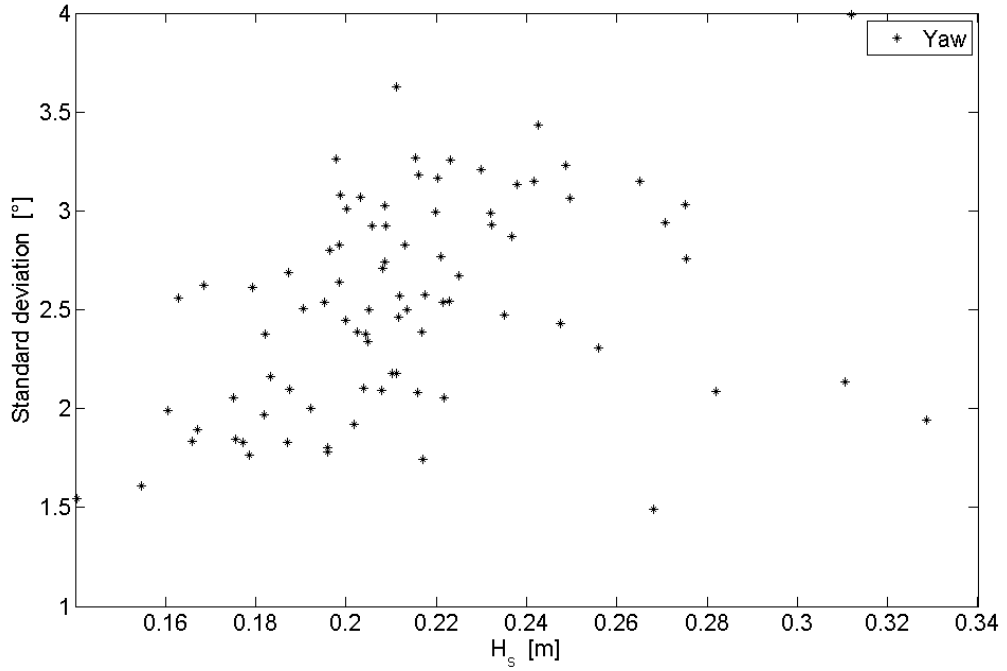


Figure 11: Significant motions in the model roll, pitch and yaw versus significant wave height.

4.3 Post processing and comparison with numerical model

The so-far recorded samples have been post-processed preliminarily to compare against the results obtained for the full scale structure. In particular, for each sea state, wave head of pressure spectra and response spectra for all degrees of freedom have been obtained, by means of Fast Fourier Transform. Each line spectrum has been then treated as described in [36] in order to obtain a function very close to the continuous spectrum, which is undetermined by nature [27].

Theoretically speaking, Response Amplitude Operators (RAOs) can be obtained in each degree of freedom as:

$$RAO_{DOF}(\omega) = \sqrt{\frac{S_{DOF}(\omega)}{S_{Wave,ph}(\omega)}} \frac{\cosh[k(d+z)]}{\cosh(kd)} \quad (6)$$

The right-handed term in Eq. 6 is due to wave attenuation due to depth at the location of wave head of pressure measurement; in particular $k(\omega)$ is the wave number, d the water depth and z the depth of the transducer. As mentioned in Section 2.1, however, peak frequencies of wave spectra are systematically in the range of [2, 3.5] rad/s. As a consequence, experimental wave spectra are not significant for frequencies far from this range. The optimal range in which RAOs could be obtained for each sea state would be $[0.5 \cdot \omega_P; 2 \cdot \omega_P]$, but natural frequencies of the model structure are lower than or close to the lower limit of this range as it can be figured out by scaling of those reported in Table 6. In order to obtain a reasonable compromise, RAOs have been calculated through Eq. (6) in the range [0.5; 4] rad/s and few records have been selected in order to minimize effects of the numerical errors in the estimation of wave spectrum at lower

and higher frequencies.

Just for the sake of comparison, in Figure 12 the experimental heave RAO and the numerical one scaled down to the model are compared. As it can be observed, good agreement is obtained close to the RAO peak frequency while a significant difference results around 1.35 rad/s, where the experimental data does not show the significant reduction, which comes from Froude-Krylov force in the linear numerical model. This evidence confirms that the model is able to catch non linear effects which are neglected by the numerical model.

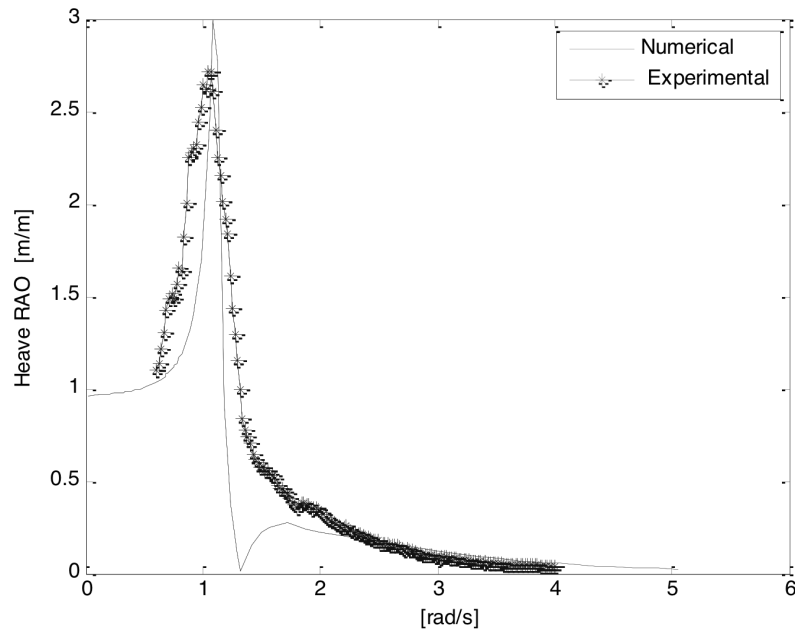


Figure 12: Heave experimental (tests performed at NOEL) VS numerical (AQWA simulations performed by authors) RAOs (mean of 9 data).

More reliable information about natural frequencies can be figured out directly from response spectra, which clearly show energy peaks close to the peak frequency of the corresponding sea state and to the natural frequencies of the model structure. The analysis of the data collected up to now shows a certain variability of natural frequencies in all the degrees of freedom; moreover the structure seems to be somehow softer than the predictions of the numerical model, with larger motions and lower frequencies. That may be due to the nonlinear dynamics of the system, which may affect numerical model reliability in ultimate load conditions. Further investigation on these experimental evidences will be carried out in the proceeding of the activity, including system identification via free decay tests, which will be performed as soon as sufficiently calm water conditions will take place.

5. Conclusions and Future Work

A 1:30 small scale field experiment, aimed to investigate dynamic behaviour of the UMaine-Hywind spar support for offshore wind turbine in severe metocean conditions has been started. Parked rotor conditions and extreme wave climate are taken into account, exploiting the favourable local sea characteristics. Furthermore, the relatively large scale allows to better represent the hydrodynamic forces and particularly the nonlinear viscous ones occurring in

severe ocean conditions.

The small scale model of the offshore wind turbine has been designed and manufactured in order to represent the prototype in Froude scale, but also structural resistance issues, relevant for the ultimate wave conditions of the site, had to be considered from a practical point of view. The mooring system has been modified due to the local inclined seabed conditions. Numerical models of the full scale and the model structure have been developed using the commercial software ANSYS AQWA and have been compared to validate the design of the latter.

The preliminary results of the experiment, obtained by processing the records collected up to now, are here presented and discussed. According to the numerical simulations, the dynamic behaviour of the model seems to be sufficiently close to that expected. Anyhow, some discrepancies have been observed, which will be investigated in the proceeding of the experimental activity, in order to try to identify the limits of the numerical model and particularly the nonlinear contributions to the structure dynamics.

In addition to collecting more data and consequently obtaining more accurate results, attention will be focused in the system identification, which is particularly challenging in a non-controlled environment. Free decay tests will be attempted, exploiting the relatively calm water conditions, systematically occurring in the site during certain months.

In the second phase of the experiment, comparative analyses will be performed to investigate the effects of the mooring system design on horizontal motions and particularly the behaviour of delta connection mooring configuration with regard to yaw. Finally, other activities are planned, such as the introduction of constant and variable forces on the top of the tower to model the aerodynamic forces imposed by the rotor, and/or different damping systems.

References

1. Failla, G. and Arena, F., New Perspectives in Offshore Wind Energy, Philosophical Transactions of the Royal Society A, 2015, 373, 20140228.
2. European Wind Energy Association, Deep Water: The Next Step for Offshore Wind Energy, European Wind Energy Association Report, Brussels, 2013. (<http://www.ewea.org>)
3. Carbon Trust, Floating Offshore Wind: Market and Technology Review, 2015 (<http://www.carbontrust.com/about-us/press/2015/06/scotland-opportunity-to-lead-floating-wind>)
4. Jonkman, J.M. and Matha, D. Dynamics of Offshore Floating Wind Turbines-Analysis of Three Concepts, Wind Energy, 2011, 14, 557-569.
5. Sclavounos P. Floating Offshore Wind Turbines, Marine Technology Society Journal, 2008, 42(2), 39-43.
6. Butterfield, S., Musial, W., Jonkman, J.M., Sclavounos, P., Engineering Challenges for Floating Offshore Wind Turbines, NREL Report No. CP-500-38776, National Renewable Energy Laboratory, Golden, USA, 2007.
7. Bachynski, E.E., Moan, T., Design Considerations for Tension Leg Platform Wind Turbines. Marine Structures, 2012, 29, 89-114.
8. Lefebvre, S. and Collu, M., Preliminary Design of a Floating Support Structure for a 5 MW Offshore Wind Turbine. Ocean Engineering, 2012, 40, 15-26.
9. Robertson, E. and Jonkman, J., Loads Analysis of Several Offshore Floating Wind Turbine Concepts, in: Proceedings of the Twenty-first International Offshore and Polar Engineering Conference, Hawaii, USA, 2011.

10. Nava, V., Soares, C.G., Arena, F., Soares C. and Pena, F., On the Assessment of Extreme Forces on a Floating Spar Wind Turbine, in: Developments in Maritime Transportation and Exploitation of Sea Resources – Proceedings of the 15th International Congress of the International Maritime Association of the Mediterranean, La Coruna, Spain, 2014, Vol. 2, 933-942.
11. Hywind Demo, 2009 (<http://www.statoil.com>)
12. Skaare, B., Nielsen, F.G., Hanson, T.D., Yttervik, R., Havmøller, O. and Rekdal, A., Analysis of Measurements and Simulations From the Hywind Demo Floating Wind Turbine. Wind Energy, 2015, 18(6), 1105-1122.
13. Jonkman, J. and Musial, W., Offshore Code Comparison Collaboration (OC3) for IEA Task 23 Offshore Wind Technology and Deployment, NREL Report No. TP-5000-48191, 2010.
14. Jonkman, J., Definition of the floating system for phase IV of OC3, NREL Report No. TP-500-47535, 2010.
15. Jonkman, J., Butterfield, S., Musial, W. and Scott G., Definition of a 5-MW Reference Wind Turbine for Offshore System Development, Report No. TP-500-38060, 2009.
16. Goupee, A.J., Koo, B.J., Kimball, R.W. and Lambrakos, K.F., Experimental Comparison of Three Floating Wind Turbine Concepts, Journal of Offshore Mechanics and Arctic Engineering, 2014, 136(2), 020906.
17. Koo, B.J., Goupee, A.J., Kimball, R.W. and Lambrakos, K.F. Model Tests for a Floating Wind Turbine on Three Different Floaters, Journal of Offshore Mechanics and Arctic Engineering, 136(2), 020907.
18. Shin, H. Model Test of the OC3-Hywind Floating Offshore Wind Turbine, in: Proceedings of the Twenty-first International Offshore and Polar Engineering Conference, Hawaii, USA, 2011.
19. Sethuraman, L. and Venugopal, V. Hydrodynamic Response of a Stepped-spar Floating Wind Turbine: Numerical Modelling and Tank Testing, Renewable Energy, 2013, 52, 160-174.
20. Viselli A.M., Goupee A.J., Dagher H.J. Model test of a 1:8 scale floating wind turbine offshore in the Gulf of Maine, in: Proceedings of the ASME 2014 33rd International Conference on Ocean, Offshore and Arctic Engineering OMAE2014, San Francisco, California, USA, 2014.
21. Jonkman, J.M. and Cordle, A. State of the Art in Floating Wind Turbine Design Tools, in: Proceedings of the Twenty-first International Offshore and Polar Engineering Conference, Hawaii, USA, 2011.
22. Skaare, B., Hanson, T.D., Nielsen, F.G., Yttervik, R., Hansen, A.M., Thomsen, K. et al. Integrated Dynamic Analysis of Floating Offshore Wind Turbines, in: European Wind Energy Conference and Exhibition, Milan, Italy, 2007.
23. Myhr, A., Maus, K.J., Nygaard, T.A. Experimental and Computational Comparisons of the OC3-Hywind and Tension-leg-buoy (TLB) Floating Wind Turbine Conceptual Designs, in: Proceedings of the Twenty-first International Offshore and Polar Engineering Conference, Hawaii, USA, 2011.
24. Gueydon, S., Xu, W. Floating Wind Turbine Motion Assessment, in: OCEANS'11 MTS/IEEE KONA, Hawaii, 2011.
25. Arena F., Ruzzo C., Strati F.M., Nava V. On the arrangement of a small scale field experiment of a spar-type support for offshore wind turbine. In: Renewable Energies Offshore, CRC Press, 657-663.
26. ANSYS ® Academic Research, Release 16.0.
27. Boccotti, P. Wave Mechanics for Ocean Engineering, Elsevier Oceanography Series, 2000.

28. Det Norske Veritas. Environmental Conditions and Environmental Loads. DNV-RP-C205. Norway, 2010.
29. Boccotti P., Arena F., Fiamma V., Barbaro G. Field Experiment on Random Wave Forces Acting on Vertical Cylinders. Probabilistic Engineering Mechanics, 2012, 28, 39-51.
30. Boccotti P, Arena F., Fiamma V., Romolo A., Two Small-Scale Field Experiments on the Effectiveness of Morison's Equation. Ocean Engineering, 2013, 57, 141-149.
31. Sarpkaya T., Isaacson M. Mechanics of Wave Forces on Offshore Structures. Van Nostrand Reinhold Co., 1981, 1-650
32. Quallen, S., Xing, T., Carrica, P., Li, Y. and Xu J. CFD Simulation of a Floating Offshore Wind Turbine System Using a Quasi-static Crowfoot Mooring-line Model, Journal of Ocean and Wind Energy, 2014, 1(3), 143-152.
33. G. K. V. Ramachandran, A. Robertson, J. M. Jonkman and M. D. Masciola. Investigation of Response Amplitude Operators for floating offshore wind turbines. Presented at the Twenty-third International Ocean, Offshore and Polar Engineering Conference, 2013, Alaska, USA.
34. ANSYS® AQWA, v. 16.0, Help System, Theory Manual, ANSYS, Inc.
35. J. S. Bendat and A. G. Piersol. Random data: analysis and measurement procedures. J. Wiley & Sons. 1986.